Modal behavior of Ti-6Al-4V specimen under high cycle fatigue

Manel Dallali, Christophe Gautrelet, Leila Khalij, Egle Conforto, Marcela Machado

Modal behavior of Ti-6Al-4V specimen under high cycle fatigue

Manel DALLALI[1], Christophe GAUTRELET[1], Leila KHALIJ[1], Egle CONFORTO[2], Marcela MACHADO[3]

[1]LMN/INSA ROUEN Normandie, Normandie université, 76000 Rouen, France.
[2]LaSIE UMR CNRS 7356, University of La Rochelle, 17042 La Rochelle, France
[3] Department of Mechanical Engineering, University of Brasilia, 70910-900, Brasilia, Brazil
manel.dalleli@gmail.com

Abstract

In this work, electrodynamic shaker was used to carry out vibration-based bending fatigue on specimens made with Ti-6Al-4V. Modal behaviour of symmetrical and unsymmetrical specimens were studied and especially the resonant frequency. This parameter makes it possible to define the rate of frequency change used to detect a change of physical properties of material due to the presence of crack for example. The impact of the geometry on the rate of frequency change is analysed and to support the analysis observations on crack growth were used to conclude on the impact of manufacturing defects.

1 Introduction

The detection of the damage in structures using the change of natural frequency is the interest of several researches. Indeed, it is known that the damage in structures can be detected by the decrease in the natural frequencies because a stiffness loss is observed with the crack growth.
The vibration-based method is one of the most used among the current techniques used in damage detection. Experimentally, the tests can be carried out with an electro-dynamic shaker especially for high cycle fatigue exploration. They make to impose complex excitations for a better behavior prediction close to real conditions in a relatively short time even close to the endurance limit. Indeed, compared to the servo-hydraulic machine, this system makes to work on a range of high frequencies and to generate an amplification of the response in the resonance zone. Therefore, the deformation response level of the specimens can be high by applying a relatively low input excitation. Thanks to this experimental setup, the resonant frequency change is used to detect when the crack appears. A rate based on the frequency drop is used by many authors to define a failure criterion. Many authors quantified the rate of frequency change to 5% in the natural frequency for the damage to be detected with confidence [1]. A recent review of the critical values adopted in the literature can be found in the paper of Xu et al. [2]. Hu et al. [3] have shown that experiments on aluminum alloy plate produced a critical value of the frequency drop of 2.8% and consider that the reduction of 5% is too rough. Xu et al. [4] and Magi et al. [5] pointed out that the sensitivity to crack propagation is not identical for all types of samples and, therefore, a single critical value of the frequency drop cannot be specified.
Therefore, we wanted to verify this observation on two kinds of specimens: symmetrical and unsymmetrical specimens made with Ti-6Al-4V material. A survey on manufacturing defects was carried out to observe the effect on the failure criterion and the fatigue life. Observations on crack growth were used to conclude on these effects, knowing that the stages of fatigue crack growth [6] are crack initiation, crack propagation and failure.

2 Vibration-based bending fatigue

2.1 Vibratory fatigue device

The experimental setup developed in the Mechanical laboratory of Normandy (LMN) is composed by an air-cooled electrodynamic shaker with an acquisition control peripheral (ACP) to control the shaker and acquire frequency signals. The detail of this setup is presented in Figure 1.

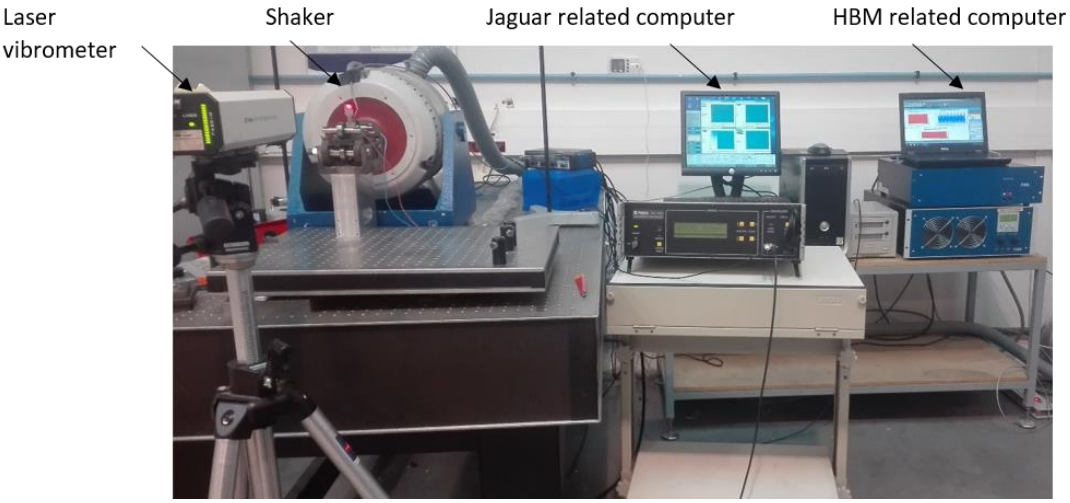

Figure 1. The vibratory fatigue bench developed in LMN [7]

The response of vibrated specimens was measured with a Polytec laser vibrometer OFV 303, positioned to the free edge and the input acceleration was measured from an accelerometer PCB 333A30 positioned on the fixture. Sweep sine tests were conducted to obtain the transmissibilities. These transmissibilities, recorded during the fatigue tests, correspond to the ratio between the output velocity and input acceleration. The time signals of input acceleration, output velocity and strain were recorded with an HBM Data Acquisition Quantum system (DAQ).
To conduct the fatigue tests, we choose to follow the resonant frequency during the fatigue tests. For this, we used the sine resonance track and dwell test (SRTD) [8,9,10]. The controller tracked automatically the resonance frequency to keep the output on resonance even if the fatigue damage causes a shift to the resonance frequency.

2.2 Focus on the specimen

In this work, Ti–6Al–4V alloy (or TA6V $\alpha\beta$ grade 5) without heat treatment material is considered. The specimens made with this material were designed in order to localize cracks far of the clamping and to reach homogeneous strain in the reduced section. One end of the specimens was clamped on the fixture designed to avoid the transversal movements [11] and the other were free. We focused the study on only the first bending mode because it leads to the higher deflection.
Ti-6Al-4V is the most used titanium alloy in aerospace and biomedical industries as a light, high strength and corrosion resistant alloy [12]. The vibration behavior of this material has been investigated by many authors especially in the additive manufacturing framework. For example, Ellyson et al. [13] and Scott-Emuakpor et al. [14] used vibratory bending fatigue to examine the behavior of Ti-6Al-4V specimens and determine the failure mechanisms. The authors conducted the studies on specimens produced respectively by selective laser melting and by direct metal laser sintering. Georges et al. [15] tested compare the behavior of three materials including the Ti-6Al-4V and showed that the experimental tests with an electrodynamic shaker were successful.
Ten samples were machined from 2 mm thickness Ti-6Al-4V plates (see Figure 2-a) according to:

- Three specimens with 80x17.6x2 (mm) dimensions were equipped with strain gages on one face of the reduced section. These samples were used for the linearity study leading to a relationship between the input acceleration and the strain measures.
- Three specimens with 80x17.6x2 (mm) dimensions were used as a reference to compare the results with unsymmetrical specimens. The resonant frequency of these specimens is approximately 345.47 Hz.
- Four specimens (denoted TC1 to TC4) were equipped with crack propagation gages HBM RDS22 (Figure 2-c and Table 1) on one face of the reduced section. Due of the machining with wire electrical discharge machine (wire-cut EDM), the dimensions vary slightly from one specimen to another and therefore contribute to modal dispersion. Especially, there is no symmetry between the two sides of the reduced section location. Thus, variability on the dimensions of the reduced section has been observed (see Figure 2-b). Therefore, we have chosen to study the effect of the variability on the modal behavior.

The measured values of the TC1 to TC4 dimensions are shown in Figure 2-a, and summarized in Table 2 with the related resonant frequencies f_r^1 corresponding to the frequency of undamaged specimens. This table shows that resonance frequency measures differ between one specimen and another due to the variability of machining.

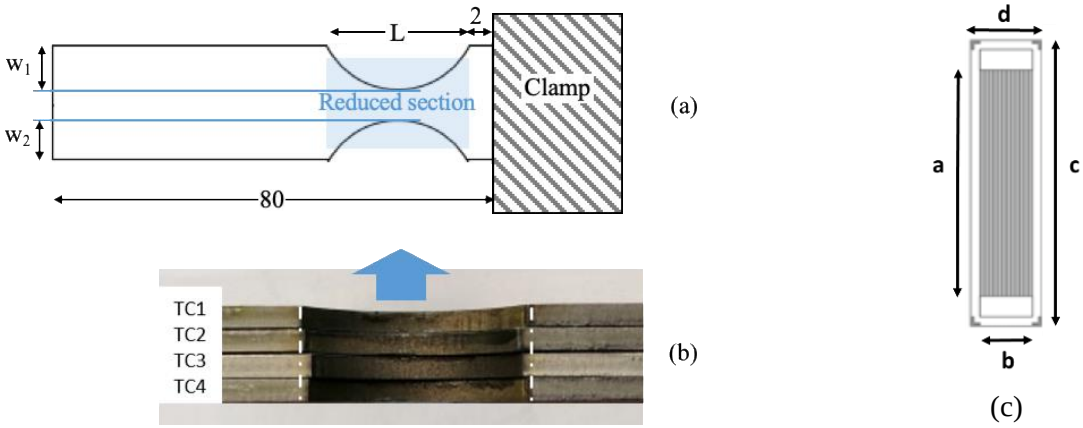

Figure 2. (a) Representation of the specimen dimension (in mm) and (b) the width variability of the reduced sections of specimens TC1 to TC4. (c) Crack propagation gauge HBM RDS22 (see Table 1)

Dimensions (mm)					
Grid length a	Grid width b	Total length c	Total width d	Distance between each link (mm)	Number of links
22	5	27.8	6.8	0.1	50

Table 1. Characteristics of the HBM RDS22 gauge

Specimen Id.	L (mm)	w_1 (mm)	w_2 (mm)	Resonant frequency f_r^1 (Hz)	Initial strain (µm/m)
TC1	79.78	5.17	5.90	332.67	1976
TC2	80.01	5.98	4.95	343.18	1905
TC3	79.61	5.76	5.03	333.87	2260
TC4	79.79	4.31	6.48	329.07	2027

Table 2. Dimensions and effect on resonant frequencies and initial strains for specimens TC1 to TC4

Density (kg/m^3)	Poisson ratio	Young's modulus (GPa)	Yield stress (MPa)
4510	0.33	108.3	786

Table 3. Mechanical properties of the Ti-6Al-4V material

The mechanical characteristics of Ti-6Al-4V are given in Table 3. The Young's modulus reported in this table was identified by the numerical model from the resonant frequency value of the reference specimen. Numerical simulation was carried out until the adjustment of the calculated and experimental values of the resonant frequency of the first mode (Figure 3).

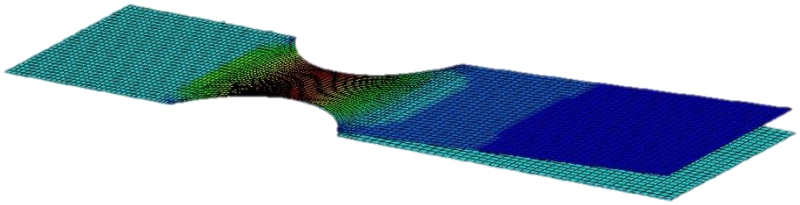

Figure 3. First Bending mode obtained from LS Dyna with elastic strain repartition

Note: The effect of the frequency was studied by Morrissey et al. [16] and Takeuchi et al. [17]. The authors showed a frequency effect on the fatigue strength when frequencies increase. However, the effect is not noticeable when the frequency remains below 400 Hz for low concentration stress and a surface fracture occurs in the smooth specimens.

2.3 Experimental procedure and data

SRTD is used in order to test specimens in fatigue. This tool allows exciting specimens at a fixed frequency that represents the system resonance. The first SRTD was conducted to obtain the resonant frequency value through a classic sweep sine. The second was carried out at this fixed frequency and an acceleration with constant level during fatigue tests. It is known in the literature that when a crack initiation occurs the resonant frequency change. The SRTD tool uses the transmissibility phase to adjust the frequency during the test and during the crack propagation.

2.3.1 Linearity study

The linearity between the excitation (amplitude of applied acceleration) and the response of the sample (the related strain measured by a gauge) was examined in order to avoid using strain gauges for fatigue tests. This linearity should make it possible to carry out fatigue tests without strain gages.
Sweep sines were performed within the frequency range [260-360] (Hz) with an acceleration range between 0.2 to 0.8 g incremented with value 0.1 and a sweep rate of 0.833Hz/sec. The first resonant frequency is included in the frequency range. An automatic procedure was used to not stop the tests. The transmissibilities and the time signals of the strain measurements recorded for each acceleration level are exhibited in Figure 4. A post-processing of the results was carried out using Matlab® to extract each value of acceleration and strain amplitudes from the ACP and DAQ files.

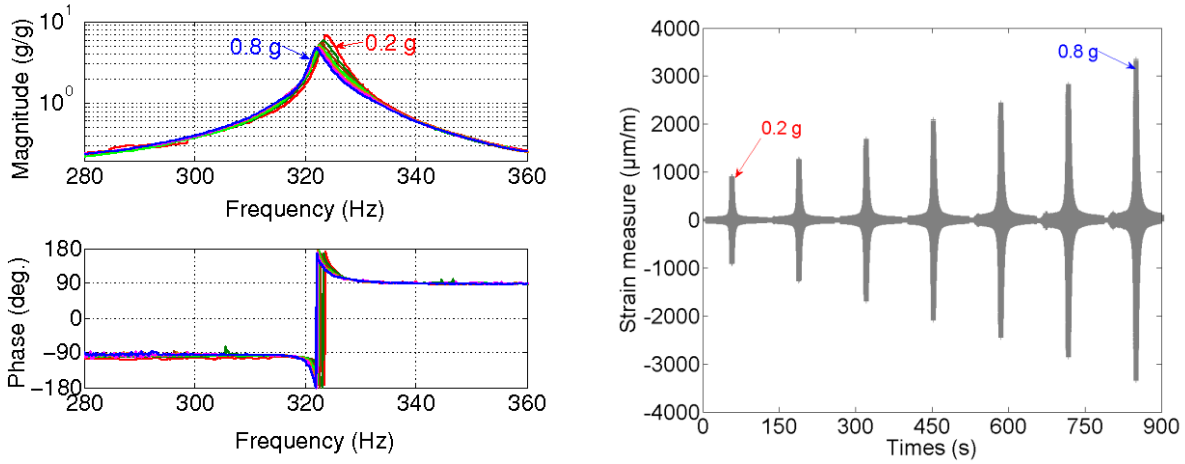

(a) (b)

Figure 4. Example of (a) transmissibility records for each acceleration levels and (b) time signals of the strain for the complete test of one specimen

Figure 5 shows the data obtained for three specimens. A linear regression from the dataset leads to a regression coefficient $R^2 = 0.985$, which suggests good proportionality between input acceleration and strain measurements. This information was used for the fatigue tests in order to choose the level of the input acceleration according to the desired strain amplitude (Table 4).

Specimen Id.	TC1	TC2	TC3	TC4
Strain amplitude (µm/m)	1976	1905	2260	2027

Table 4. Initial strain obtained from linearity approach

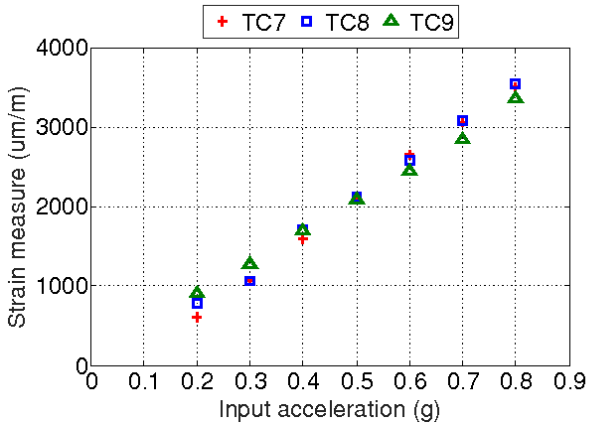

Figure 5. Linearity results for three specimens

2.3.2 Effect of the crack growth on the transmissibilities

In general, the damage of metallic materials under both static and dynamic loading is related to only one failure mechanism, corresponding to the initiation and propagation of one or multiple cracks on the surface. The main objective of this part is to study the effect of the crack growth on the transmissibilities of the reference specimens. The manufacturing of these specimens led to symmetrical reduced sections.

The fatigue test was carried out on the three specimens TC10 to TC12 excited with a swept sine vibration within a frequency range between 260 to 360 Hz. The procedure flowchart of the test is presented in Figure 6. $p = 1$ corresponds to the transmissibility recording for the undamaged specimen. The test was carried out until the resonance frequency drop reached the threshold of 15% (denoted p_c in the flowchart) with a step set at 1% decrease.

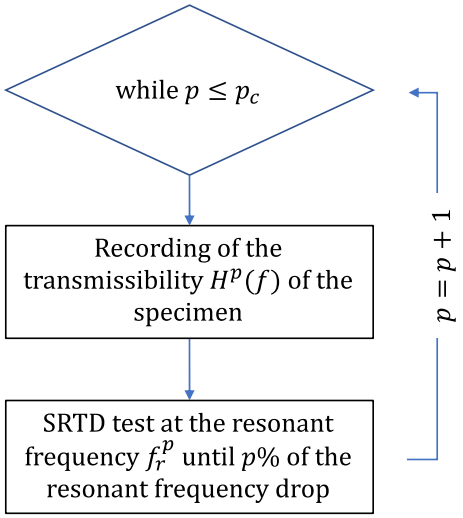

Figure 6. Procedure flowchart of the test

Figure 7-a represents the records of the p-th transmissibilities related to the resonant frequency drops followed by the SRTD. This behavior was observed for the three specimens but only one specimen result is presented. We can observe a shift to the left of the transmissibilities during the fatigue crack propagation and particular shapes of the magnitude corresponding to non-linearity of the specimen response due to the crack presence. This non-linearity is clearly visible when two transmissibility magnitudes are superimposed (Figure 7-b top). The transmissibilities were recorded for one sweep direction explaining the non-complete peak of resonance. The non-linear behavior of the Ti-6Al-4V was highlighted by Georges et al. in [15] which evoke instability of the response. The phase behavior at 15% supports this observation (Figure 7-b bottom). The two-phase microstructure of Ti-6Al-4V material ($\alpha\beta$) may explain this behavior. Ongoing SEM (scanning electron microscope) analysis is expected to provide a better understanding of the impact of this microstructure.

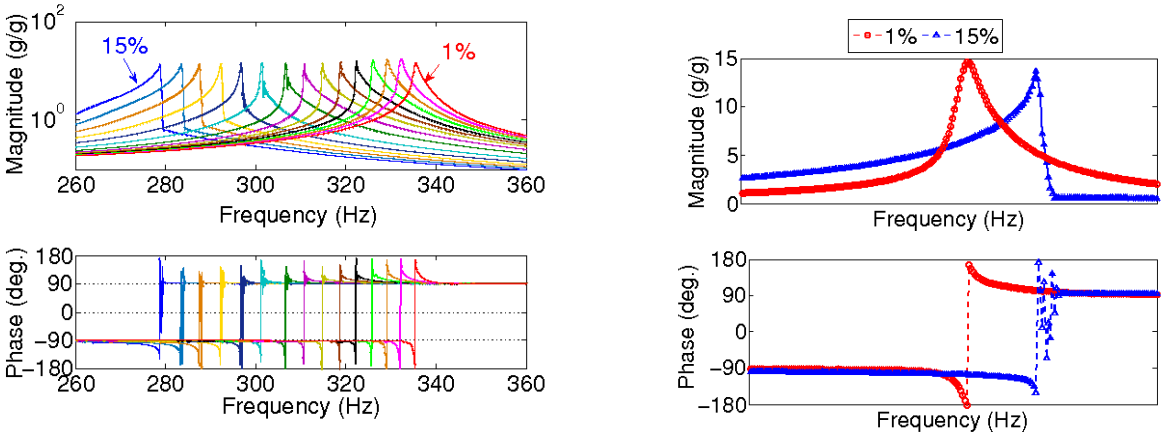

(a) (b)

Figure 7. (a) Magnitude and phase of the transmissibilities recorded during a fatigue test of one specimen and (b) focus on superimposition of two magnitudes and phases

A fluorescent dye penetrant with ultraviolet light was used to observe the fracture site in the reduced section. The inspection revealed two parallel cracks that probably indicate growth in two opposite directions (Figure 8). The fracture severity is responsible of the response instability and therefore explains the behavior of the transmissibility.

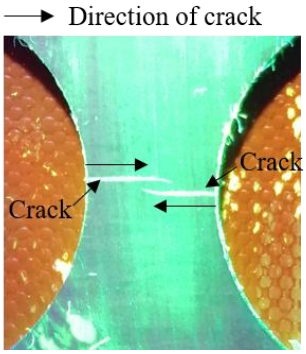

Figure 8. Observation of crack with dye penetrant inspection of symmetric specimen

3 Effect of geometric variabilities

The effect of geometric variation on the crack growth was studied in this part.

Fatigue tests were conducted on 4 unsymmetrical specimens in order to characterize the effect of the geometry on the damage. Crack propagation gauges RDS 22 were used to follow the crack growth. This one gradually increases the electrical resistance of the gauge as the crack continues to extend [18].

SRTD tool was used to track the resonance until the fracture. Data acquisition was performed using HBM Catman measurement software (DAQ) and the ACP. The resonant frequencies were recorded during the fatigue test by the ACP and the time signals of accelerometer, velocity and gauge were measured by the DAQ system. The tests were performed until the breaking of the crack propagation gauge leading to infinite value of strength.

It is known that the specimens have not experienced complete separation during vibration-based bending tests, the crack lengths may be measured, in contrast to axial tests with conventional fatigue tests for example [4,20]. Therefore, the crack length measurement via dye penetrant with ultraviolet light is carried out after each fatigue test.

Figure 9-a gives a representation in time-frequency (spectrogram) of the time signal of the input acceleration to compute the short-time Fourier transform of a signal. The resonant frequency values were extracted from this spectrogram and plotted versus the cycle number in Figure 9-b. The resonant frequency drop is clearly visible during the fatigue test.

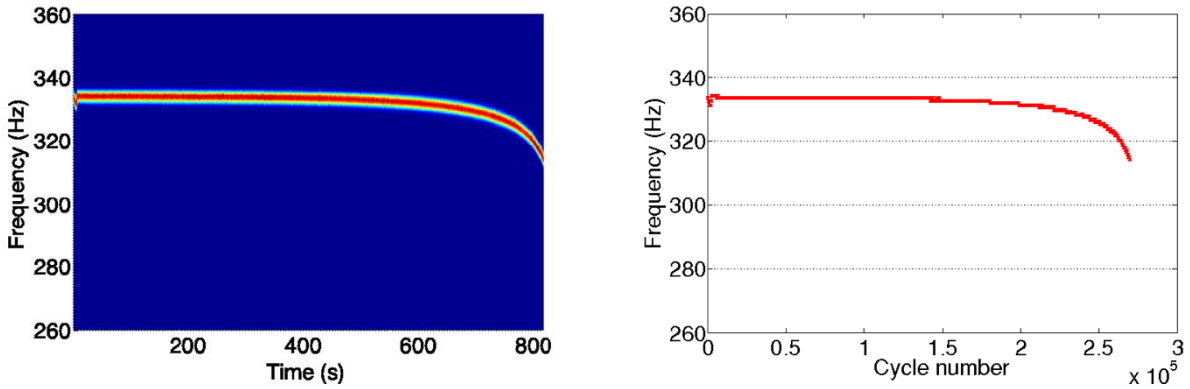

(a) (b)

Figure 9. (a) Time-frequency representation of the time signal of the input acceleration and (b) resonant frequency evolution vs cycle number of the specimen TC3

In addition, the crack length (denoted a) obtained from the crack propagation gauges is plotted against the cycle number (Figure 10-a). It reveals three slopes: the first horizontal straight line corresponds to the undamaged specimen; the slow slope change can be identified as the moment when one or more macro-cracks initiated while the last slope represents the instability of the fracture. These three slopes can be related to the three stages of the fatigue crack growth corresponding to the opening mode (mode I). The fatigue lives corresponding to the total lives, were extracted from each curve of Figure 10-a and reported in Table 5. Nevertheless the cycle number to crack initiation denoted N_f was not obtained from the same curves because of the difference between the total length and grid length of the RDS 22 gauges (see Figure 2-c and Table 1). This shift induces a late detection of crack initiation.

Schijve [19] defines the fatigue life as the addition of the initiation period and the crack growth period. The author found that more than 90 % of the fatigue life is spent before cracks are usually detectable under high-cycle fatigue conditions. Bruns et al. [20] showed that the dynamic changes were perceptible on average at 60% of the fatigue life. The authors defined a failure criterion by a sudden drop in the resonant frequency which considered as an indication of crack initiation. The change rate of frequency was analyzed to relate the significant changes in the rate to initiation and fracture. Many authors such as Paulus [21], Paulus et al. [22], Habtour et al. [23] used the change rate of frequency as a damage index that compares the p-th resonant frequency denoted f_r^p with the one that follows denoted f_r^{p+1}. The p-th ($p = 1. \ldots . m$) resonant frequency is obtained for the N-th fatigue cycle applied to the structure. $p = 1$ corresponding to the undamaged structure. This parameter is also defined as the rate of the frequency change (RFC) given by:

$$\%\mathrm{RFC} = \frac{f_r^1 - f_r^p}{f_r^1} \times 100 \tag{1}$$

It should be noted that this gauge does not provide information on the number of crack initiation site. As to SRTD tool, RFC criterion gives the resonant frequency drop during the fatigue cycle. Figure 10-b investigates the relationship between the crack length and RFC values and Table 5 summarized the main results. P(%) represents the proportion of the fatigue life due to crack initiation and N_f was obtained from the slope change of the resonant frequency curves of Figure 9-b. Each surface of the specimen reduced sections was inspected with the dye penetrant.

From these graphs and table, we can observe that:

(1) The propagation behavior of crack from one specimen to another is different.
(2) The RFC of TC4 is higher than RFC of the other specimens even so its fatigue life is close to that the TC2 specimen. For almost the same fatigue life, the resonance frequency drop is longer therefore the crack propagation is slower.
(3) TC4 has only one crack site while two are present for the others (see Table 5).
(4) TC1 and TC3 reached almost the same fatigue life but their RFC differ.

(2) and (3) lead to conclude that the fracture time with one crack is slower than two cracks. It is simple common sense. From the observations of (1) and (4), we can conclude that the difference in geometry does not necessarily lead to a large difference in fatigue life.
If we confront the results obtained from symmetrical and unsymmetrical specimens, we can observe that the symmetry leads to the same crack lengths on each side of specimen. Indeed, the crack length measurements of Figure 8 give 4.48 mm on the left side and 4.08 mm on the right side. Unlike, the crack lengths differ for the unsymmetrical specimen. The crack initiated and propagated on the side w_2 of TC4 which can be considered as the highest stress concentration zone because the difference in dimension with w_1 is not negligible (see Table 2). In our opinion this case may explain the observation (3). TC2 presents a small crack (1.5 mm) on side w_1 (5.98 mm) and a larger crack (3.8 mm) on side w_2 (4.95 mm). The difference in dimensions w_1 and w_2 is small but it doesn't explain the difference of crack length observed on each side of TC2.

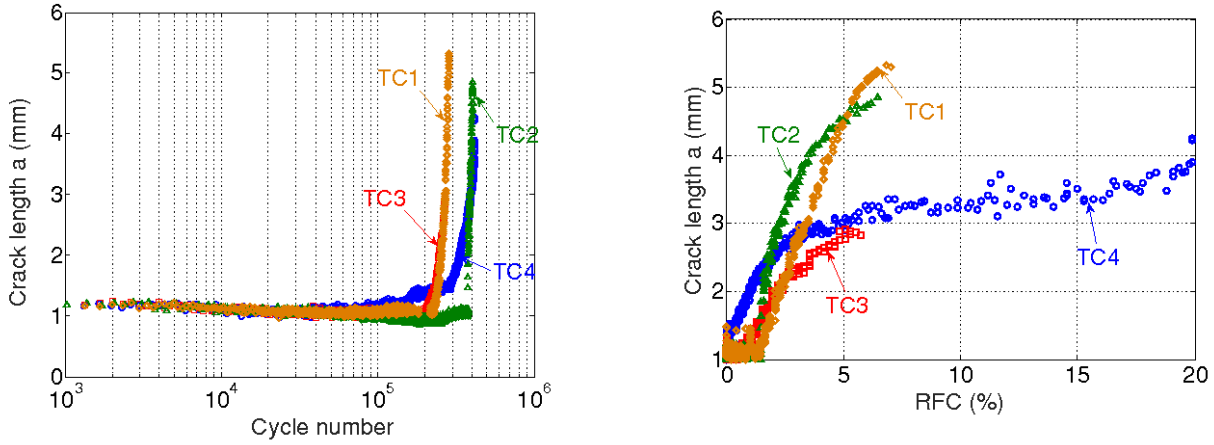

(a) (b)

Figure 10. Crack length (a) versus cycle number and (b) versus RFC

Specimen Id	Initiation			Failure			
	N_f ($\times 10^5$)	RFC (%)	P(%)	RFC (%)	Fatigue life ($\times 10^5$)	a (mm)	Crack number on one face
TC1	1.76	0.82	60.98	7.1	2.87	5.3	2
TC2	2.83	0.15	69.02	6.5	4.10	4.8	2
TC3	1.53	0.22	57.09	5.7	2.68	2.8	2
TC4	2.67	0.28	63.57	20	4.20	4.3	1

Table 5. Result summary of the tests on unsymmetrical specimens

Regarding the RFC criterion of each specimen, we can observe that the RFC value for crack initiation is very low compared to the values provided by the literature. Nevertheless, the fraction of life P is consistent with the results obtained by Bruns et al. [20] for all specimens.

4 Conclusion

This paper presents a vibration-based experimental study on specimens made with Ti-6Al-4V. The main objective of this study was to demonstrate the impact of the manufacturing defects on the vibratory fatigue behavior. Ti-6Al-4V is a complex material and the response in vibration shows a non-linearity even an instability for damaged structure. To quantify the relevance and study the strain rate effects, further investigations are needed, especially with a higher number of specimens.

5 Acknowledgements

This study was conducted within the framework of the project MADNESS. which has been funded with the support from the European Union with the European Regional Development Fund (ERDF) and from the Regional Council of Normandie.

6 Reference

[1] Salawu, O., 1997. Detection of structural damage through changes in frequency: a review. Engineering Structures, 19(9), pp. 718-723.
[2] W. Xu, X. Yang, B. Zhong, G. Guo, L. Liu, C. Tao. Multiaxial fatigue investigation of titanium alloy annular discs by a vibration-based fatigue test. Int J Fatigue 2017;95:29–37.
[3] H-T. Hu, Y-L. Li, T. Suo, F. Zhao, Y-G. Miao, P. Xue, Q. Deng. Fatigue behavior of aluminum stiffened plate subjected to random vibration loading. Trans. Nonferrous Met. Soc. China 2014;24:1331−1336.
[4] W. Xu, X. Yang, B. Zhong, Y. He, C. Tao. Failure criterion of titanium alloy irregular sheet specimens for vibration-based bending fatigue testing. Engineering Fracture Mechanics 2018;195:44–56.
[5] F. Magi, D. Di Maio, I. Sever. Validation of initial crack propagation under vibration fatigue by Finite Element analysis. International Journal of Fatigue 2017;104:183–194.
[6] Naser, J. M., & Serrano Toledano, F. (2011). Analysis of vibration-induced fatique cracking in steel bridges.
[7] L. Khalij, Christophe Gautrelet, Alain Guillet. Fatigue curves of a low carbon steel obtained from vibration experiments with an electrodynamic shaker. Materials and Design 2015;86:640–648.
[8] Rouillard V, Sek MA. A frequency domain technique for maintaining resonance condition during sine dwell vibration testing of packages. Packag Technol Sci. 2000;13:227-232.
[9] Minderhoud J. Improving SRTD testing with resonance phase settings. Sound Vib. 2013;47:13-15.
[10] Su, Q, Pitarresi, J, Gharaibeh, M, Stewart, A, Joshi, G, Anselm, M. Accelerated vibration reliability testing of electronic assemblies using sine dwell with resonance tracking. 2014 IEEE 64th Electronic Components and Technology Conference (ECTC), Orlando, FL. 2014; 119–125.
[11] Appert, A., Gautrelet, C., Khalij, L., & Troian, R. (2018). Development of a test bench for vibratory fatigue experiments of a cantilever beam with an electrodynamic shaker. In *MATEC Web of Conferences* (Vol. 165, p. 10007). EDP Sciences.
[12] Leyens, C. and Peters, M. (2003). Titanium and Titanium Alloys, Fundamentals and applications.
[13] Ellyson, B., Brochu, M., & Brochu, M. (2017). Characterization of bending vibration fatigue of SLM fabricated Ti-6Al-4V. *International Journal of Fatigue*, *99*, 25-34.
[14] Onome Scott-Emuakpor, Casey Holycross, Tommy George, Kevin Knapp and Jeffery Bruns. Fatigue and Strength Studies of Titanium 6Al-4V Fabricated by Direct Metal Laser Sintering. ASME Turbo Expo 2015: Turbine Technical Conference and Exposition Volume 6: Ceramics; Controls, Diagnostics and Instrumentation; Education; Manufacturing Materials and Metallurgy; Honors and Awards Montreal, Quebec, Canada, June 15–19, 2015.
[15] George TJ, Seidt J, Shen M-HH, Nicholas T, Cross CJ. Development of a novel vibration-based fatigue testing methodology. Int J Fatigue 2004;26(5):477–86.
[16] Morrissey, R. J., McDowell, D. L., & Nicholas, T. (1999). Frequency and stress ratio effects in high cycle fatigue of Ti-6Al-4V. *International Journal of Fatigue*, *21*(7), 679-685
[17] Takeuchi, E and Furuya, Y and Nagashima, N and Matsuoka, S (2008). The effect of frequency on the giga-cycle fatigue properties of a Ti–6Al–4V alloy. Fatigue & Fracture of Engineering Materials & Structures, 31(7), 599–605.
[18] https://disensors.com/product/rds-crack-propogation-gauges/
[19] Schijve, J. (1979). Four lectures on fatigue crack growth: I. Fatigue crack growth and fracture mechanics. Engineering Fracture Mechanics, 11(1), 169-181.
[20] J. Bruns, A. Zearley, T. George, O. Scott-Emuakpor, C. Holycross. Vibration-based bending fatigue of a hybrid insert-plate system experimental Mechanics 2015;55:1067–1080
[21] Paulus, M. E. (2011). Fatigue damage accumulation due to complex random vibration environments: application to single-axis and multi-axis vibration (Doctoral dissertation).
[22] Paulus, M., Dasgupta, A., & Habtour, E. (2012). Life estimation model of a cantilevered beam subjected to complex random vibration. Fatigue & fracture of engineering materials & structures, 35(11), 1058-1070.
[23] Habtour, E., Paulus, M., & Dasgupta, A. (2014). Modeling approach for predicting the rate of frequency change of notched beam exposed to Gaussian random excitation. Shock and Vibration, 2014.